Presented at the 41st European Photovoltaic Solar Energy Conference and Exhibition, 23-27 September 2024, Vienna, Austria

EFFECT OF LOWERING CURING TEMPERATURE OF ELECTRICALLY CONDUCTIVE ADHESIVES ON RIBBON CONNECTED SOLAR CELLS

Veronika Nikitina, Tim Riehle, Leonhard Böck, Torsten Rößler
Fraunhofer Institute for Solar Energy Systems ISE, Heidenhofstraße 2, 79110 Freiburg, Germany
Corresponding Author: Veronika Nikitina | +49 761 4588 2199 | e-mail: veronika.nikitina@ise.fraunhofer.de

ABSTRACT: Electrically conductive adhesives (ECAs) can be used for the interconnection of temperature-sensitive solar cells like perovskite-silicon tandem (PVST) due to their low processing temperatures. This study investigates the impact of lowering the ECA curing temperatures ≤ 140 °C on the volume resistivity, the cell interconnection quality, and the long-term stability under thermal cycles. With ECA interconnection, additional silver in the module is introduced. This work estimates the total silver consumption in PVST modules and explores possible routes for its reduction. Replacement of Ag interconnector coating with Sn is investigated in terms of long-term stability under damp heat and joint resistance. Variation of tested ECAs included products with 17, 60, 70 and > 70 wt% silver, to realize a detailed study of the silver content effect on volume resistivity, joint resistance, module performance and interconnection reliability. Silver consumption in PVST module was estimated to be 168 mg per M6 cell, corresponding to ~24 mg Ag/W. Joint resistance with tin was observed to be higher than with silver, corresponding to –0.2 $\%_{rel.}$ P_{MPP} loss attributed to series resistance in a PVST module. No increase in joint resistance with ECA interconnected tin-coated ribbons after 3000 h in damp heat was observed. Volume resistivity as well as module performance after lamination was found to profit from higher ECA silver content. ECA processing temperature was found to influence the performance of the interconnection differently for each ECA. However, longer curing time resulted in higher fill factor and better long-term stability for all tested products.

Keywords: low-temperature interconnection, electrically conductive adhesives, perovskite-silicon tandem, module technology

1 INTRODUCTION

Electrically conductive adhesives (ECAs) are increasingly used in the photovoltaic industry to interconnect temperature sensitive solar cells or in combination with the shingle [1,2] technology.

ECAs consist of a polymer matrix with conductive particles (fillers) [3], which typically consist entirely or partially of silver. Upon curing of the polymer, conductive paths are formed. In the photovoltaic industry, thermal curing of the ECAs is common, where the assembled string is heated to a processing temperature [4].

Advantages of ECAs include their versatility [5–10], the ability to tailor the product characteristics for specific applications [11–13], interconnection geometry flexibility (metallization not necessarily required), and low processing temperatures (down to 80 °C). The latter makes ECA interconnection a suitable method for perovskite-silicon tandem (PVST) solar cells. However, a drawback of using ECAs is the increased silver consumption and the limited availability of data regarding long-term stability.

PVST is a rapidly developing cell technology. Its current record for power conversion efficiency (PCE) stands at 34.6 % on a laboratory device [14] and 30.1 % on an M6 (166 mm × 166 mm) cell [15]. PVST cells are expected to enter the market after 2025 with a PCE of ~26 % [16]. Besides their high PCEs and steep learning curve, PVST cells have approximately half the current density (J_{SC}) compared to PERC, TOPCon or SHJ cells [17], which could help reducing the module power loss (ΔP_{MPP}) due to series resistance (R_S). Challenges associated with PVST cells regarding interconnection and module encapsulation are their moisture and temperature sensitivity [18]. This requires adjustments to the processing temperatures, bill of materials (BOM) and module design.

This study investigates the impact of lowering the curing temperature of ECAs on the performance and long-term stability of interconnection and the pathways to drastically reduce silver consumption in PVST modules.

2 METHODS

2.1 Silver Consumption in PVST Modules and Reduction Strategies

We estimate the silver consumption in various components of a PVST module and investigate strategies to reduce it, including the use of tin-coated interconnectors, ECAs with low silver content, and busbarless cell interconnection.

To estimate the silver consumption, we used published data and technical data sheets. The calculation is based on the input parameters provided in Table I.

Table I: Input parameters for the calculation of the silver consumption in a PVST module. It is assumed that the ECA is applied at the metallization pad positions.

	Value	Ref.
Wafer size	166 mm × 166 mm	-
Number of fingers, front	60	[19]
Number of fingers, rear	120	[20]
Finger width	25 µm	[21]
Finger height	8 µm	[22]
Number of busbars (BB)	6	[23]
Width of a line connecting BB pads	100 µm	[24]
Number of pads per BB	12	-
Mean pad area	1.4 mm^2	-
BB height	20 µm	-
ECA density	4.2 g/cm^3	TDS
ECA Ag content	17 wt%	TDS
Ribbon width	0.5 mm	-
Ribbon coating thickness	1 µm	TDS

2.3 Electrical characterization

The difference in anodic indexes between two metals (–0.15 V and –0.65 V for Ag and Sn, respectively) may lead to galvanic corrosion of a less noble one (Sn) in a joint. However, in the environment of a solar module using encapsulation materials with very low water vapor transmission rate this scenario is highly unlikely. To study the hypothesis, that the encapsulation polymer in a PVST module design acts as a sufficient barrier to isolate Ag/Sn contacts, joints (Fig. 1) consisting of Sn-coated ribbons interconnected with an ECA-2 were fabricated and aged in damp heat for 3000 h (85 % RH and 85 °C for 3000 h). Sample preparation included printing the ECA using a stencil with dimensions of 0.1 mm × 1 mm × 2 mm. The assembled joints were cured on a hot plate at 140 °C for 5 min. After curing, the samples were laminated with polyolefin (POE) foil at 150 °C for 20 min in a glass-glass setup. Two variations were prepared: with butyl-based edge seal and without one. Joint resistance was measured both after production and after aging in DH3000.

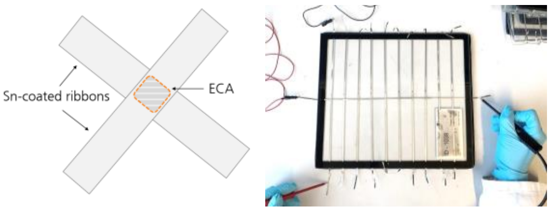

Figure 1: Sample design (left) and measurement (right) for the investigation of the Sn/Ag joint galvanic corrosion.

In order to examine how the replacement of Ag with Sn in the ribbon coating influences the joint resistance (R_{joint}), we used the method described by Böck et al. [25]. Printed circuit boards (PCB) with Ag and Sn surfaces were utilized to mimic ribbon coating. Samples with four ECAs (Tab. II) were cured in the dry convection oven for 30 min at 100 °C, 110 °C, 120 °C, 130 °C and 140 °C. Chosen ECAs have different silver content and can be cured at temperatures ≤ 140 °C. The range of the tested temperatures lays above the curing reaction point of each ECA and within the processing temperature range of PVST cells. Processing temperature may influence the curing behavior of the ECA (polymer contraction, evaporation of additives) and, as a result, volume resistivity.

After curing of the PCBs, joint resistances (R_{joint}) were measured. Subsequently, samples were laminated at 160 °C for 10 min with Teflon foil to simulate the solar module lamination process and measured again.

The PCBs design furthermore allows measuring volume resistivity ($R_{\mathrm{vol.}}$) of the ECAs, which may vary dependent on the curing scheme, silver content and polymer chemistry [11].

Table II: ECAs used in this work. “DSC” refers to differential scanning calorimetry, dynamic measurement with 10 K/min ramp [26].

	ECA-1	ECA-2	ECA-3	ECA-4
Polymer matrix	A	B	B	B
Density [g/cm^3]	4.4	4.2	3.0	2.4
Filler type	Ag	Cu/Ag	Ag	Ag
Ag content [wt%]	> 70	17	70	60
DSC curing peak [T °C]	85	98	89	88

2.4 Performance in the module

To evaluate the effect of curing temperature on the quality of the cell interconnection, small-scale solar modules were fabricated. The interconnection was carried out on a TT1600ECA stringer [27] with an integrated screen printer for ECA application. Strings with two half-cells were produced with industrial M6 (166 mm × 83 mm) busbarless silicon-heterojunction (SHJ) cells. Due to the absence of busbar metallization, ECAs were printed continuously to ensure proper electrical connection between fingers. The ECA print width accounted to 0.4 mm at the front and 0.6 mm at the rear side, 5 busbars were printed. The busbar amount was dictated by the constraints of the production equipment and does not represent an optimal value. This ECA application design resulted in 40 mg, 119 mg, and 82 mg silver per M6 wafer for ECA-2, ECA-3 and ECA-4, respectively. The utilized ECA printing pattern represents an unoptimized design, where the focus is laid on expected sufficient long-term stability. This was done in order to study the curing scheme effect without possible additional influences of ECA reduction. ECA-1 was not used in the module performance investigation due to processing difficulties. Severe printing defects (line interruption) were observed after 3 h on screen, worsening with time. We assume it is associated with the low pot life (6 h) of the material. The ECAs were cured using schemes considered compatible with the industrial interconnection of PVST cells, with temperatures up to 140 °C and curing times of up to 90 seconds, while recognizing that these parameters may vary depending on specific material and process requirements. Silver-coated interconnectors with a light reflective structure at the sunny side with 1.0 mm × 0.2 mm cross-section was used. The lamination was performed in a plate-membrane laminator at 150 °C for 20 minutes. The samples’ stack consisted of front glass (3.2 mm), POE encapsulation foil and white polyethylene (PET) backsheet with an additional aluminum layer. Given the number of samples (180), the glass-backsheet design was chosen to simplify the sample logistics. It is not expected that the used encapsulation BOM will have a major effect on the experiment results.

To assess the long-term stability of the interconnection and its possible dependency on the curing scheme, small-scale modules were subject to 200 cycles in an accelerated thermocycling chamber (aTC200), where the ambient temperature was varied between –40 °C and +85 °C with a rate of 8 K/min and dwell times of 10 min [28]. During the accelerated thermocycling the components of the joint experience contraction and expansion according to their thermal expansion coefficients (CTE). Aging the small-scale modules with aTC helps understanding if the combination of materials and processes results in an interconnection which will be stable during operation under changing environmental conditions.

Characterization of the small-scale modules after production and after aTC200 included visual examination, current-voltage (I-V) measurement and electro-luminescence (EL) imaging. The combination of these three methods allows the most efficient evaluation of the interconnection quality. Visual inspection was used to check for the macroscopic degradation features (change in color, appearance of corrosion or gas inclusions etc.). Using *I-V* measurement, electrical characteristics of the small-scale modules like short-circuit current (I_{SC}), open-circuit voltage (V_{OC}), fill factor (*FF*) and maximum power point (P_{MPP}) can be examined. I_{SC} represents optical effects, V_{OC} allows tracking the possible cell damage, *FF* reflects the series resistance losses and, as a result, interconnection quality. P_{MPP} encompasses the influence of all the above. EL images facilitate the *I-V* data interpretation by revealing local cracks, interconnection defects or cell degradation.

Figure 2: Small-scale solar module fabricated for this study, with a total of 180 modules produced (10 modules per group).

3 RESULTS AND DISCUSSION

3.1 Silver consumption in a PVST module

Considering the input parameters given in the table I, the following silver use was estimated (Tab. III).

Table III: Calculated silver consumption per PVST cell (M6, 6 busbar design) for metallization (contact fingers and busbar) and interconnection (ECA and interconnectors)

	Ag [mg/cell]
Fingers	60
Busbars	75
ECA	7
Interconnector	26
Total	**168**

For a 60-cell PVST Module of 421 W [29], total silver consumption of 168 mg/cell accounts to ~24 mg Ag/W (metallization and interconnection) of which ~19 mg Ag/W is attributed to the metallization. This corresponds to the silver use in TOPCon cells (19 mg Ag/W) and is ~5 mg Ag/W lower than for SHJ (24 mg Ag/W) [14].

3.2 Electrical characterization

After the exposure to DH3000, no significant change in the R_{joint} of Sn-coated ribbons interconnected with ECA-2 was observed (Fig. 3). Samples laminated with POE only (no edge seal) also demonstrated no increase in $R_{joint.}$ The latter implies that POE module encapsulation either served as a sufficient barrier from the moisture ingress or that the moisture diffused through the module edges did not cause joint degradation.

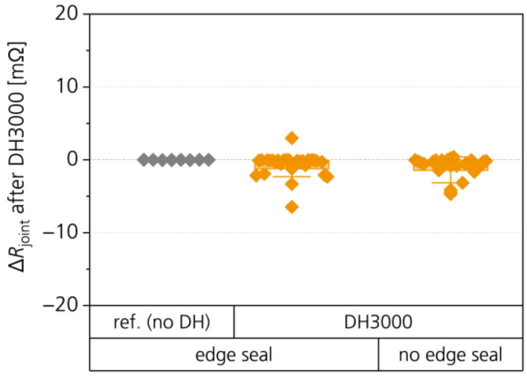

Figure 3: Difference between the initial R_{joint} (after curing and lamination) and R_{joint} after DH3000 for modules with and without edge sealing. Per sample group, 30 measurements were performed. One datapoint represents one measurement.

The results of the joint resistance measurements are presented in Figure 4. Joints with Sn-coated PCBs overall demonstrate higher resistance. However, the values with Sn are acceptable for the interconnection of the PVST cells. Taking the module design from sections 2.1 and 3.1 into account, joint resistances of 10 mΩ and 100 mΩ would result in –0.2 $\%_{rel.}$ and –1.6 $\%_{rel.}$ P_{MPP} loss attributed to R_S, respectively. A larger contact area would correspond to lower ohmic losses (not shown in Fig. 4).

Strong data scattering prevents from recognizing trends connected with ECA curing temperature. Values obtained after curing did not differ considerably from the presented data in Figure 4.

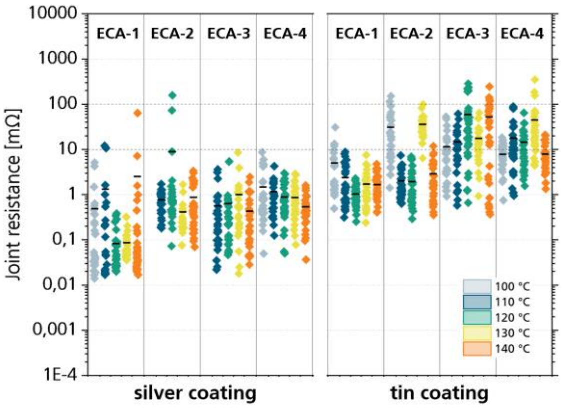

Figure 4: Results of the joint resistance measurement after curing at different temperatures and lamination of the PCBs. Per group, 19 to 57 measurements were performed. One datapoint represents one measurement.

The results of the volume resistivity measurements are shown in Figure 5. Overall, the tested ECAs exhibit different values, which correspond to their composition. Those with higher silver content show lower $R_{vol.}$ After curing (Fig. 5, transparent boxes), temperature-dependent behavior is evident with ECA-1, where samples cured at 100 °C demonstrate the median value of 2.5×10^{-4} Ω·cm, and the samples cured at 140 °C show significantly lower median of 3.0×10^{-5} Ω·cm. ECA-2 and ECA-3 show slightly higher $R_{vol.}$ for samples cured at 100 °C.

After lamination, the $R_{vol.}$ reduced strongly with

ECA-1, evening out the median values for various curing temperatures to ~1×10^{-5} Ω·cm. ECA-3 and ECA-4 behave alike, where groups cured at lower temperatures (100 °C, 110 °C) show $R_{vol.}$ decreasing after lamination. This may be due to the incomplete curing in the convection oven and reaction completion during lamination. The lower the oven temperature was, the more pronounced the effect appears. ECA-2 does not follow a particular trend: samples cured at 100 °C show the decreasing $R_{vol.}$ whereas with other groups the $R_{vol.}$ increases by ~2×10^{-3} Ω·cm (140 °C) to ~6×10^{-3} Ω·cm (130 °C). For all three polymer B-based materials (Tab. III) lowest $R_{vol.}$ was achieved through curing at lowest temperature with subsequent lamination. In general, all considered ECAs demonstrate volume resistivity values compatible with solar cell interconnection.

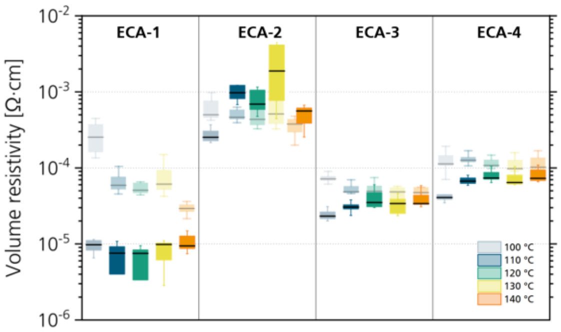

Figure 5: Results of the volume resistivity measurement after curing (transparent) at different temperatures and lamination (full color) of the PCBs. One box plot is represented by 10 measurements. Black lines refer to median values.

3.3 Performance in the module

Results of the *I-V* characterization of small-scale modules are given in Figure 6. The fill factor is shown as this parameter depends on the series resistance and can be evaluated as an indication for the interconnection performance. Initial *FF* of the cell accounted to 80.9 % (not shown in Fig. 6).

Median of the cell-to-module (CTM) loss in *FF* varies from –6.2 $\%_{rel.}$ (ECA-3, cured 90 s at 100 °C) to −11.4 $\%_{rel.}$ (ECA-2, cured 45 s at 130 °C). Depending on the curing scheme, each ECA behaves differently after lamination (Fig. 6, transparent boxes):

- ECA-2 shows higher *FF* if cured slower at lower temperatures (–8.6 $\%_{rel.}$ and –10.6 $\%_{rel.}$ for 90 s at 120 °C and 45 s at 140 °C, respectively).
- ECA-3 exhibits slightly higher median values at lower curing temperatures independent of the curing time (–6.2 $\%_{rel.}$ and –6.9 $\%_{rel.}$ for 100 °C and 140 °C, respectively).
- ECA-4 demonstrates a distinct increase in *FF* from 130 °C upwards (–6.4 $\%_{rel.}$ and –10.4 $\%_{rel.}$ for curing 90 s at 130 °C and 90 s at 120 °C).

After exposure to aTC200 (Fig. 6, full color boxes), *FF* decreases in all groups to a different extent. General trends highlighted in the previous paragraph endure. Least degradation is observed with ECA-2, in samples cured 90 s at 120 °C. They show median *FF* loss (relative to the module performance after lamination) of –1.2 $\%_{rel.}^{aTC}$. ECA-3 demonstrates lowest degradation at lowest curing temperature (ΔFF of –2.5 $\%_{rel.}^{aTC}$, cured 90 s at 100 °C). However, higher median value for the group cured for 90 s at 130 °C than neighboring groups (120 °C and 140 °C, both for 45 s) indicates, that increasing curing time may improve the long-term stability of the interconnection. The latter is consistent with ECA-4, where increasing curing time from 45 s to 90 s results in ΔFF improvement from −5.7 $\%_{rel.}^{aTC}$ to –3.7 $\%_{rel.}^{aTC}$. Longer curing results in a higher achieved degree of curing (DoC) which could have facilitated the long-term stability of the interconnection.

No differences between groups or systematic degradation features were observed in EL images or during the visual inspection of the small-scale modules.

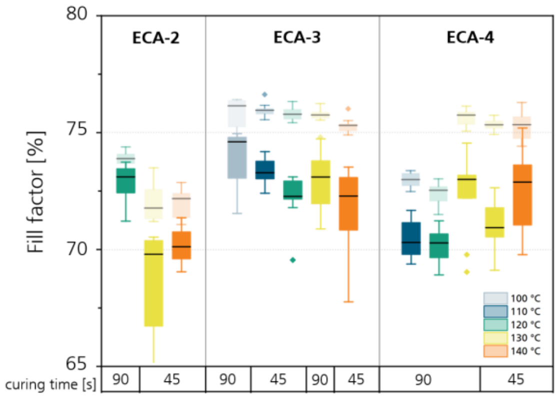

Figure 6: Fill factor of the small-scale modules measured after lamination (transparent) and aTC200 (full color). One box plot is represented by 10 samples. Black lines refer to median values.

4 SUMMARY

In this study, the use of ECAs for the interconnection of PVST cells is reviewed. The main focus lays on investigating the effect of low curing temperatures (≤ 140 °C) on interconnection quality. Additionally, the silver consumption in various components of a PVST module is estimated and three strategies to minimize Ag usage are explored: replacement of silver interconnector coating with tin, ECAs with low silver content, and busbarless interconnection. Tests were performed with four ECAs with different chemistry, including varying Ag content. The following key findings were acquired in this study:

- Silver consumption in PVST module was estimated to be ~19 mg Ag/W (metallization only) and ~24 mg Ag/W (metallization and ECA interconnection).
- No increase in R_{joint} in Sn/Ag-based ECA/Sn joints encapsulated in POE was observed after DH3000.
- R_{joint} is higher for the Sn coated surfaces. However, all values are compatible with the PVST cell interconnection: replacing Ag coating with Sn would results in ~0.2 $\%_{rel.}$ P_{MPP} loss in a PVST module.
- ECAs with higher Ag content show lower $R_{vol.}$ After curing, ECA-1 (polymer type A, > 70 wt% Ag) exhibits lower values at higher T°C, which even out and decrease to

~$1\times10^{-5}\,\Omega\cdot$cm after lamination. For all 3 polymer B-based materials lowest $R_{vol.}$ was achieved through curing at lowest temperature (100 °C) with subsequent lamination. In general, all considered ECAs demonstrate volume resistivity values compatible with solar cell interconnection ($<10^{-2}\,\Omega\cdot$cm).

- The *FF* of small-scale modules with busbarless SHJ cells varied based on used ECA and curing conditions. For each ECA, different behavior after lamination was observed. Samples with ECA-2 and ECA-3 showed less *FF* loss at lower curing T °C, whereas ECA-4 demonstrated distinct improvement in *FF* from 130 °C onwards. After aTC200 the positive effect of longer curing time on long-term stability of the interconnection is observed.

5 OUTLOOK

This study highlights the impact of curing conditions on the performance of low-temperature ECA interconnection. The findings suggest that optimizing curing parameters can enhance module performance and long-term stability. Additionally, the feasibility of replacing Ag interconnector coating with Sn was demonstrated, particularly in terms of joint resistance and stability under damp heat conditions, presenting a promising route to reducing Ag consumption in solar modules. The automatic interconnection process ≤ 140 °C and ≤ 90 s was successfully implemented using busbarless SHJ cells, which further contributes to lowering silver usage.

Future research should focus on exploring the effects of combining the Sn-coated interconnectors, low-Ag ECA and busbarless metallization grid in a low-temperature ECA interconnection process.

REFERENCES

[1] N. Abdel Latif, et al., 40th European Photovoltaic Solar Energy Conference and Exhibition (2023).
[2] T. Roessler, et al., Proceedings of the 10th Metallization and Interconnection Workshop (2022) 20012.
[3] T. Geipel. Electrically Conductive Adhesives for Photovoltaic Modules, Fraunhofer ISE, Freiburg, 2017 // 2018.
[4] T. Geipel, et al. (2019).
[5] T. Geipel, et al., Photovoltaics International 21 (2013).
[6] DELO Industrial Adhesives. Product overview. https://www.delo-adhesives.com/us/products/bonding/overview-of-adhesives.
[7] Henkel Adhesive Technologies. Electricall conductive adhesives. https://www.henkel-adhesives.com/de/en/products/industrial-adhesives/electrically-conductive-adhesives.html.
[8] Panacol-Elosol. Technical data sheets. https://www.panacol.com/products/data-sheets#elecolit.
[9] Polytec Polymere Technologien. Two-component conductive epoxies. https://www.polytec-pt.com/int/electrically-conductive/products/2-component-conductive-epoxies.
[10] B. ROARTIS bvba. Electrically condictive adhesives (isotropic). https://www.iq-bond.com/electrically-conductive-adhesives-isotropic/.
[11] F. Tan, et al., International Journal of Adhesion and Adhesives 26 (2006) 406–413.
[12] M.R. Sanghvi, et al., Polymer Bulletin 79 (2022) 10491–10553.
[13] H. Derakhshankhah, et al., Journal of Materials Science: Materials in Electronics 31 (2020) 10947–10961.
[14] LONGI. 34.6%! Record-breaker LONGi Once Again Sets a New World Efficiency for Silicon-perovskite Tandem Solar Cells, 2024. https://www.longi.com/en/news/2024-snec-silicon-perovskite-tandem-solar-cells-new-world-efficiency/.
[15] LONGI. LONGi announces the new world record efficiency of 30.1% for the commercial M6 size wafer-level silicon-perovskite tandem solar cells, 2024. https://www.longi.com/en/news/is-m6-wafer-silicon-perovskite-tandem-cells-new-efficiency-record/.
[16] VDMA Photovoltaic Equipment. International Technology Roadmap for Photovoltaic (ITRPV), 2023. itrpv.vdma.org.
[17] Y. Zhang, et al., Energy & Environmental Science 14 (2021) 5587–5610.
[18] A.u. Rehman, et al., Progress in Photovoltaics: Research and Applications 31 (2021) 429–442.
[19] V. Nikitina, et al., Solar Energy Materials and Solar Cells 263 (2023) 112590.
[20] S. Pingel. Pers. communication, 2024.
[21] A. DeRose, et al., Solar Energy Materials and Solar Cells 261 (2023) 112515.
[22] S. Pingel, et al., Solar Energy Materials and Solar Cells 265 (2024) 112620.
[23] C. Messmer, et al., Progress in Photovoltaics: Research and Applications 30 (2022) 374–383.
[24] TongWei Solar Energy Co., Ltd. TW Solar Energy HJT 166 9B Silicon Heterojunction Solar Cells TW166Y209.
[25] L. Böck, et al., Proceedings of the 14th International Conference on Crystalline Silicon Photovoltaics 2024.
[26] Deutsches Institut für Normung e. V., Prüfung von Kunststoffen und Elastomeren; Thermische Analyse; Dynamische Differenzkalorimetrie (DDK). Prüfung von Kunststoffen und Elastomeren; Thermische Analyse; Dynamische Differenzkalorimetrie (DDK).
[27] https://www.teamtechnik.com/.
[28] Schiller C. et al., Proceedings of the 36th European Photovoltaic Solar Energy Conference and Exhibition (2019) 995–999.
[29] Fraunhofer ISE / Oxford PV. Oxford PV and Fraunhofer ISE develop full-sized tandem PV Module with record efficiency of 25 %, 2024. https://www.ise.fraunhofer.de/en/press-media/press-releases/2024/oxford-pv-and-fraunhofer-ise-develop-full-sized-tandem-pv-module-with-record-efficiency-of-25-percent.html.